Solvent-modulated Binding Selectivity of Reaction Substrates to Onium-based σ-Hole Donors

Alexandra A. Sysoeva,[1] Alexander S. Novikov,[1] Dmitrii S. Bolotin[1]*

[1] Institute of Chemistry, Saint Petersburg State University, Universitetskaya Nab. 7/9, Saint Petersburg, 199034, Russian Federation

* Corresponding author E-mail: d.s.bolotin@spbu.ru

Combination of experimental data and results of DFT calculations indicates that the catalytic activity of chalconium and halonium salts served as σ-hole donating organocatalysts cannot be clearly estimated via analysis of the electrostatic potential on the catalysts' σ-holes and values of the catalyst···TS intermolecular interactions, such as polarization effects, charge transfer, or covalency of bonding. Moreover, the real catalytic effect might not correlate well with the values of Gibbs free energies of activation of the reactions, because solvation effects and other competitive binding processes play at least the same or even more important role in the catalysis. It was showed in present work, that the solvation either can lead to the increase of equilibrium concentration of reactive catalyst···electrophile associates thus accelerating the reaction or brings favorable generation of catalyst···nucleophile species resulting in suppression of the catalytic activity of the organocatalyst.

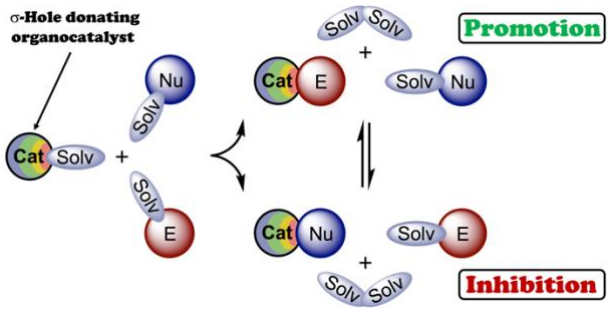

Introduction

Today, σ-hole donating species binding to reaction substrates via chalcogen (ChB) or halogen (XB) bonds—interactions between electron-deficient chalcogen or halogen atom and a Lewis base, respectively[1, 2]—play an important role in noncovalent organocatalysis,[3, 4] as they provide more directional orientation and higher electrophilic activation of ligated species compared with traditional hydrogen bond (HB)[5, 6] donating organocatalysts.[7, 8] ChB and XB donors also exhibit very low sensitivity to oxygen and water and thus have benefits toward many metal-containing Lewis acids.[9, 10] Considering this, wide dissemination of ChB and XB donors into the fields yet utilizing traditional HB donating organocatalysts,[10-13] as well as metal-based Lewis acids, can provide the evolution of sustainable catalysis in the direction of application of efficient and environmentally benign catalytic species.

The σ-hole donating organocatalysts exhibit similar general trends in catalytic activity, which implies its increasing from lighter to heavier σ-hole carriers[14] and thereby the compounds featuring electron-deficient tellurium and iodine elements were shown to exhibit the highest catalytic activity among ChB[2, 15, 16] and XB[17-19] bond donors. Moreover, the cationic organocatalytic species have significantly higher activity compared to the uncharged compounds.[8, 20-27] Recently, it was shown that cationic chalcogen(IV)- or halogen(III)-derived σ-hole donors (chalconium and halonium salts; **Figure 1**) are remarkably more active than their chalcogen(II)- and halogen(I)-containing analogues. Thus, iodonium salts featuring two σ-holes at the iodine atom exhibit higher catalytic activity than

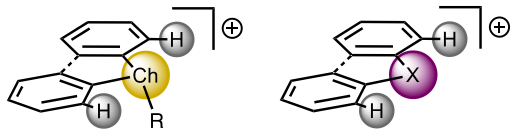

Chalconium cation Halonium cation

Figure 1. Chalconium and halonium species as highly catalytically active ChB- and XB-donating organocatalysts.

cationic iodine(I)-based catalysts[28] and effectively catalyze a wide range of organic reactions.[29-43] Similarly, telluronium salts featuring three σ-holes at the tellurium atom represent a higher catalytic activity than that of tellurium(II) derivatives and lighter chalcogen(IV)-derived species.[44, 45]

Although onium salts were shown to catalyze a wide range of reactions, there is no single point of view on the nature of the electrophilic activation of reaction substrates by these species. Thus, in our previous work it has been concluded that the dominant factor of decreasing of the Gibbs free energy of activation is polarization of a transition state provided by the organocatalysts, whereas a charge transfer as well as covalency of the catalyst···substrate interaction has negligible effect.[41] Another work[46] represents oppositional view on this question and suggest that the substrate-to-catalyst charge transfer plays the dominant role. Whatever the factors providing the electrophilic activation of a substrate, it is possible only when this substrate is ligated to the organocatalytic species. During the reaction progress, the catalyst can reversibly bind not only to the target electrophile (**Scheme 1**, ***a***), but also to the nucleophilic agents and/or intermediates and a reaction product

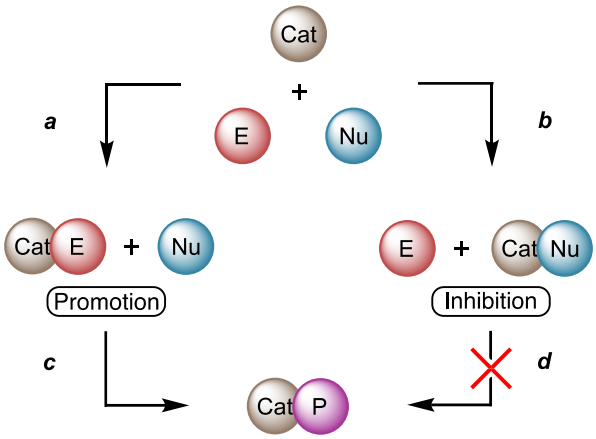

Scheme 1. Competitive routes of the catalyst···substrate binding.

(**Scheme 1**, ***b***).[40, 42] These competitive processes should be considered since all of them are able to decrease the catalytic activity of the σ-hole donor. In the extreme case, if the catalyst predominantly binds to the nucleophile, the catalytic effect can be completely suppressed, and the reaction rate even can be reduced due to decrease of equilibrium concentration of unbound nucleophilic species.

In this work, we decided to shift the focus of the discussion from the nature of electrophilic activation to the less obvious but likely more important binding factor. Recently we suggested a reliable model for consideration of the binding process during DFT calculations[47] and here we apply this model onto estimation of the solvent effects for the systems involving onium salt catalysis to shed light on how the nature of the solvent affects the equilibrium concentration of reactive catalyst···electrophile associates. Based upon the experimental and theoretical study on the catalytic activity of a series of onium salts in different solvents, discussion of the factors affecting their catalytic activity related to the binding processes is represented.

Results and Discussion

Selection of onium salts and their catalytic activity in a model reaction. Onium cations are potentially reactive toward nucleophilic agents, owing to their tendency to form uncharged chalcogen(II)- and halogen(I)-containing species.[43, 48-51] Considering that the noncovalent organocatalysts must retain their chemical structure during the reaction progress, fully arylated onium salts has been chosen in this study, because they are less reactive toward nucleophilic agents than their alkyl, vinyl, alkynyl, and other counterparts. Taking into account that halonium salts containing condensed aryl rings are more acidic[50] and exhibit higher catalytic activity[40, 42] than their acyclic analogues, and considering that iodonium salts exhibit higher catalytic activity and stability toward nucleophilic species than their bromonium and chloronium congeners,[52] dibenziodolium triflate **Cat3**^{OTf} has been chosen as a representative example of XB donor. Among ChB donors, the dibenzothiophene and dibenzoselenophene derivatives (**Cat1**^{OTf} and **Cat2**^{OTf}, respectively), featuring two condensed phenyl rings, were selected as structural analogues of **Cat3**^{OTf} (**Scheme 2**). The telluronium salts are not considered in this study due to their low stability against the elimination of elemental tellurium.[53]

As a model reaction, Schiff base formation has been chosen. Reaction of *tert*-butyl amine with 4-methyl benzaldehyde in CD_3CN, $(CD_3)_2SO$, or CD_3OD at 25 °C leads to a reversible formation of the Schiff base 4-TolC(H)=N^{t}Bu (**Scheme 2**). ^{1}H NMR monitoring indicated that this reaction proceeds slowly in the aprotic solvents when non-catalyzed. Availability of 10 mol % of **Cat1**^{OTf} or **Cat2**^{OTf} provides no observable catalytic effect in $(CD_3)_2SO$, whereas remarkable rise of the reaction rate has been detected in CD_3CN. In CD_3OD, the non-catalyzed reaction proceeded significantly faster than that performed in the aprotic media; no catalytic effect was observed for **Cat2**^{OTf}, but **Cat1**^{OTf} exhibited low but perceptible acceleration of the reaction. **Cat3**^{OTf} provided significant acceleration of the model reaction in all the solvents, but the highest acceleration was detected in CD_3CN.

All these qualitative observations clearly indicate that the catalytic effect of the σ-hole donating catalysts significantly depend on the reaction media and the solvent plays an important role in the process of catalysis, since it can totally suppress the activity of some of the organocatalytic species or, vice versa, allow the catalyst to show outstanding activity.

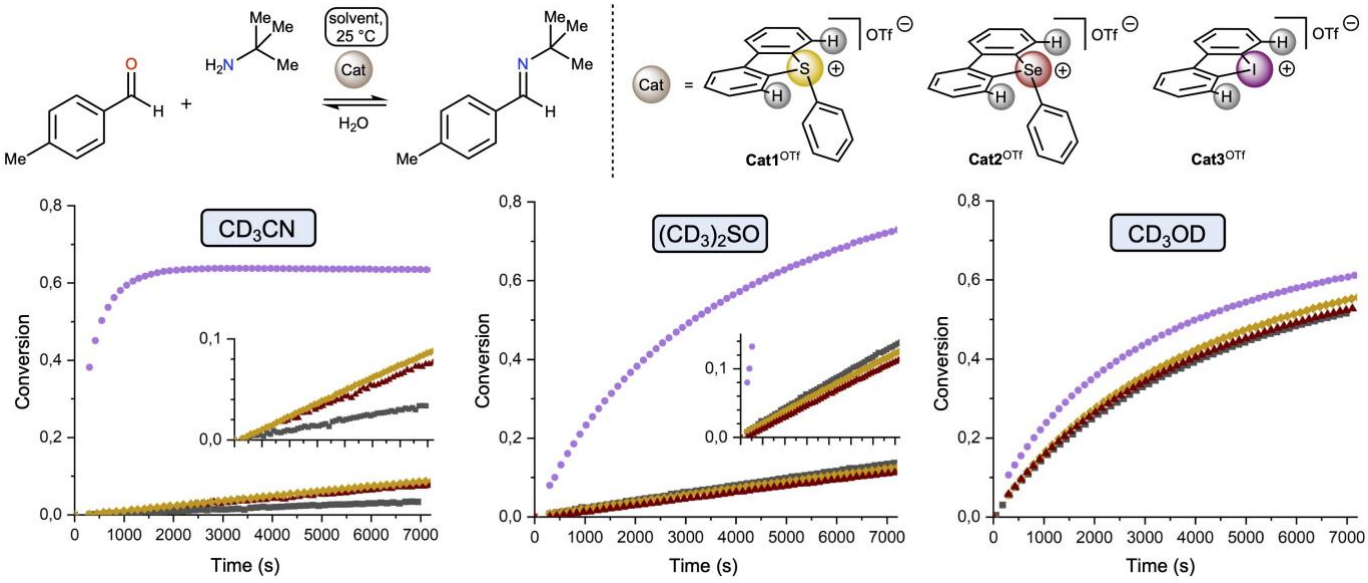

Scheme 2. Structures of the selected catalysts **Cat1**^{OTf}–**Cat3**^{OTf}, model reaction and ^{1}H NMR monitoring of its progress in the presence of the catalysts (10 mol %) and their absence. Yellow — **Cat1**^{OTf}, red — **Cat2**^{OTf}, purple — **Cat3**^{OTf}.

Quantitative analysis of the kinetic data. To obtain quantitative benchmarks for further compare with DFT calculations, the forward and reverse reaction rate constants were calculated based on the ^{1}H NMR monitoring data. The equilibrium constant K for the model reaction can be written as the following equation (**eq. 1**):

$$K = \frac{k_1}{k_{-1}} = \frac{x_{eq}(x_{eq}+d_0)}{(a_0-x_{eq})^2} \qquad \text{eq. 1}$$

where k_1 is the rate constant of the forward reaction (M^{-1} s^{-1}), k_{-1} is the rate constant of the reverse reaction (M^{-1} s^{-1}), x_{eq} is equilibrium concentration of the imine (M), a_0 is starting concentration of the aldehyde (M), d_0 is starting concentration of water (M). The concentration-vs-time dependence can be linearized (**Figure 2**) by the following equation in coordinates $\ln\frac{x-x_{eq}}{x-x^*_{eq}}$ vs t:

$$\ln\frac{x-x_{eq}}{x-x^*_{eq}} = (k_1 - k_{-1})(x_{eq} - x^*_{eq})t + ln\frac{x_{eq}}{x^*_{eq}}, \qquad \text{eq. 2}$$

where $x^*_{eq} = \frac{2Ka_0+d_0}{K-1} - x_{eq}$

$$\begin{cases} k_1 = \frac{SK}{(x_{eq}-x^*_{eq})(K-1)} \\ k_{-1} = \frac{S}{(x_{eq}-x^*_{eq})(K-1)} \end{cases}, \quad \text{where} \quad S = (k_1 - k_{-1})(x_{eq} - x^*_{eq})$$

is the slope of the line. eqs. 3–4

Solution of the obtained equations by the least squares method led to the values of k_1 and k_{-1} (**Table 1**). Due to very low conversion, no precision calculation of the constants was possible for the non-catalyzed and catalyzed by the **Cat1**^{OTf} and **Cat2**^{OTf} reaction in CD_3CN or $(CD_3)_2SO$. Rough estimation of the reaction rates in these solvents gave k_1^{MeCN}~10^{-5} M^{-1} s^{-1}, k_{-1}^{MeCN}~10^{-6} M^{-1} s^{-1}, k_1^{DMSO}~10^{-4} M^{-1} s^{-1}, k_{-1}^{DMSO}~10^{-7} M^{-1} s^{-1}.

The k_1 and k_{-1} values clearly indicate that **Cat1**^{OTf}–**Cat3**^{OTf} have a significant effect on the rate of both forward and reverse reactions. In CD_3OD, **Cat3**^{OTf} serves as a typical Lewis acid and expectedly increase the k_1 and k_{-1} values (entries 1 and 4), whereas the effect of **Cat1**^{OTf} and **Cat2**^{OTf} turned out to be not so predictable since they have almost no effect on the forward reaction rate but *inhibit* the reverse reaction (entries 1–3). This observation can be explained in terms of dominant binding of **Cat1**^{OTf} and **Cat2**^{OTf} with H_2O molecules served as a nucleophile in the reverse reaction (imine + H_2O → aldehyde + amine). Selective ligation of H_2O also might explain their negligible catalytic effect on the forward reaction, because of occupation of the coordination vacancies of the S and Se centers in **Cat1**^{OTf} and **Cat2**^{OTf}, respectively, which prevent binding of the catalysts with the electrophile.

Table 1. The calculated from the experimental kinetic data forward and reverse reaction rate constants in CD_3CN, $(CD_3)_2SO$, or CD_3OD for **Cat1**^{OTf}–**Cat3**^{OTf}.

Entry	Solvent	Catalyst	K	$k_1\times10^3$ (M^{-1} s^{-1})	$k_{-1}\times10^5$ (M^{-1} s^{-1})
1	CD_3OD	–	26	1.1	4.3
2	CD_3OD	**Cat1**^{OTf}	51	1.2	2.3
3	CD_3OD	**Cat2**^{OTf}	32	1.1	3.6
4	CD_3OD	**Cat3**^{OTf}	34	1.7	5.1
5	CD_3CN	**Cat3**^{OTf}	10	13	130
6	$(CD_3)_2SO$	**Cat3**^{OTf}	1800	2.2	0.12

Density functional theory calculations for determination of the relative binding energies. For computational analysis of the **Cat**$^+$···substrate association process, we used the model suggested by us previously,[47] because it gave the results similar with experimentally obtained binding energies. This model assumes involvement in computations of two solvent molecules taken in the explicit form: one ligated to the catalyst σ-hole and another bound to the nucleophilic part of a reaction substrate (**Figure 2**). The Gibbs free energies of binding were calculated for a series of the most abundant solvents, which are typically utilized in organic syntheses (i.e. THF, Me_2SO, MeCN, DMF, Pyridine, $CHCl_3$, H_2O, and MeOH; **Table 2**).

The data indicate that **Cat1**$^+$ predominantly binds with the aldehyde in each solvent taken for the consideration, but the relative ratio between equilibrium concentrations of **Cat1**$^+$···**A** and **Cat1**$^+$···**B** species—depending on the $\Delta G_{binding}$(**A•Cat**)–$\Delta G_{binding}$(**B•Cat**) value (**Figure 2**)—has significant differences. For the **Cat2**$^+$ and **Cat3**$^+$ species, the **Cat**$^+$···**B** is dominant form in THF, Me_2SO, and MeCN, whereas the **Cat**$^+$···**A** associates prevail in the other chosen solvents. On the one hand, this observation indicates that rational choice of the solvent for the catalyzed reaction can lead to the significant increase of equilibrium concentration of the activated form of an electrophile, making the most of the catalyst in the reaction. On the other hand, poor choice of the solvent can lead to the total inhibition of the catalytic effect due to complexation of a nucleophilic species to the catalyst.

Density functional theory calculations for determination of the Gibbs free energy of activation of the model reaction. DFT calculations of the Gibbs free energy of activation of the first step of the modelled reaction were carried out to better understand an impact of the association process on the reaction rate. In the model applied for the calculations, the 6-membered transition states were chosen.

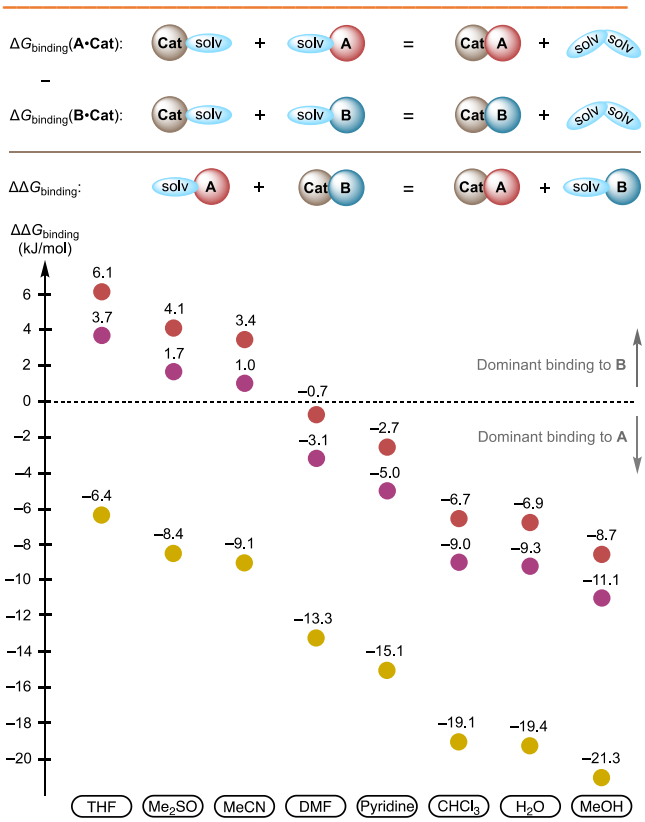

Figure 2. Schematic representation of the binding process and difference in the calculated energies of binding with **Cat1**$^+$–**Cat3**$^+$ between the aldehyde (**A**) and amine (**B**). Yellow — **Cat1**$^+$, red — **Cat2**$^+$, purple — **Cat3**$^+$.

Table 2. The calculated Gibbs free energies of binding for **Cat1**$^+$–**Cat3**$^+$ with the aldehyde (**A**) or amine (**B**) in a series of solvents.

Solvent	1		2		3	
	$\Delta G_{binding}$ (**A•Cat**)	$\Delta G_{binding}$ (**B•Cat**)	$\Delta G_{binding}$ (**A•Cat**)	$\Delta G_{binding}$ (**B•Cat**)	$\Delta G_{binding}$ (**A•Cat**)	$\Delta G_{binding}$ (**B•Cat**)
THF	1.2	7.6	4.2	–1.9	2.1	–1.6
Me_2SO	–8.1	0.3	4.2	0.1	1.2	–0.5
MeCN	–4.4	4.7	–8.0	–11.4	–2.5	–3.5
DMF	1.7	15.0	3.1	3.8	5.0	8.1
Pyridine	4.4	19.5	11.3	14.0	9.3	14.3
$CHCl_3$	–15.8	3.3	–27.8	–21.1	–34.7	–25.7
H_2O	–9.9	9.5	–11.8	–4.9	–12.1	–2.8
MeOH	–9.3	12.0	–8.2	0.5	–13.1	–2.0

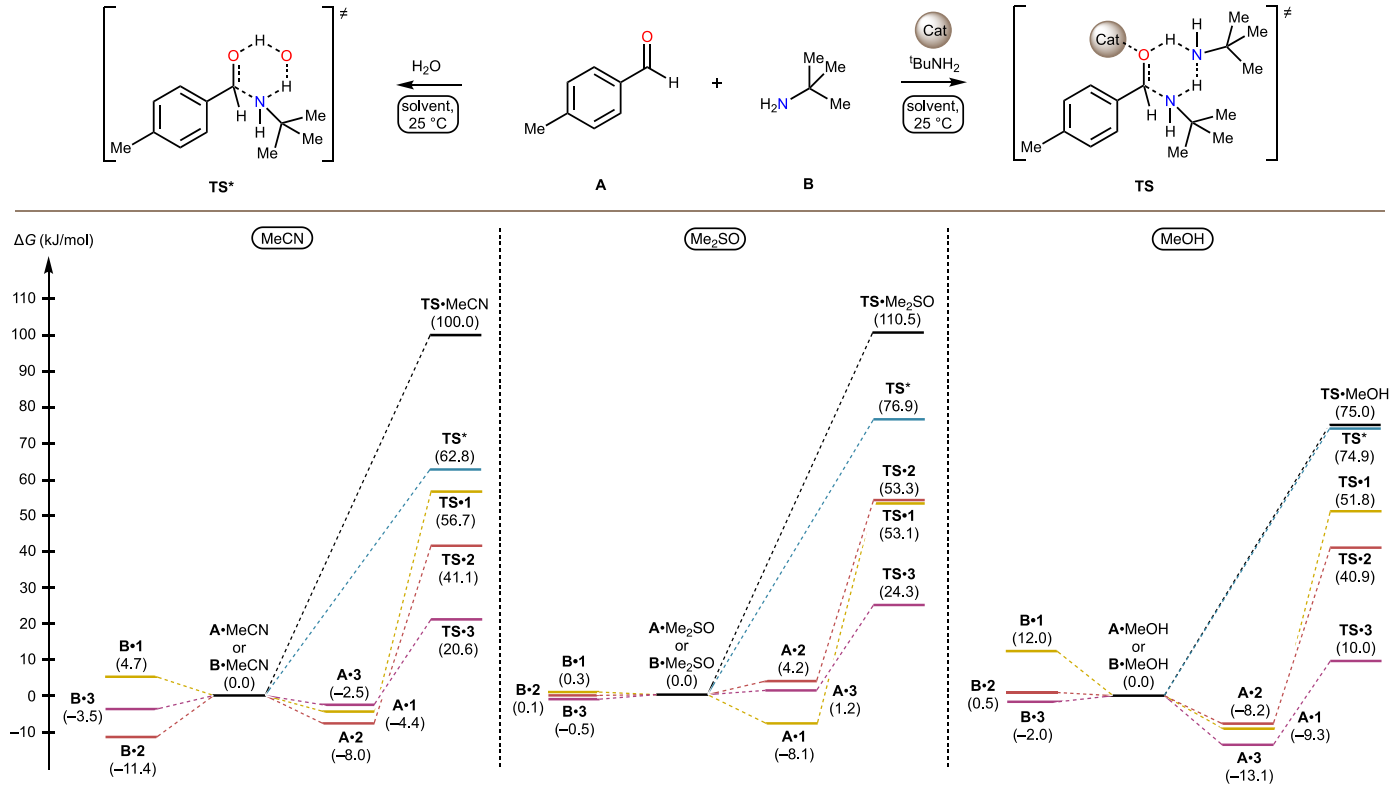

Scheme 3. The calculated energy profiles for the aldehyde–amine coupling reaction.

One of them involved two molecules of the amine (**TS**),[54, 55] whereas another involved one molecule of the amine and H_2O molecule (**TS***)[56] since all the solvents utilized for the ^1H NMR monitoring contained traces of water and H_2O is also eliminated in the progress of the reaction (**Scheme 3**).

In all chosen solvents (MeCN, Me_2SO, and MeOH), the iodolium cation **Cat3**$^+$ carrying significantly more positive electrostatic potential on its σ-holes[14, 42, 55] than the sulfonium and selenonium cations (**Cat1**$^+$ and **Cat2**$^+$, respectively) expectedly exhibited the highest reduction of the Gibbs free energy of activation. Nevertheless, all the catalytic species have been indicated by the results of DFT calculations should provide significant catalytic effect, which experimentally was not detected for **Cat1**^{OTf} and **Cat2**^{OTf} in Me_2SO, whereas in MeCN and MeOH, the effect was significantly lower than that estimated from the calculations. This may indicate that their catalytic activity was reduced by the complexation with the reaction substrates different from the electrophilic aldehyde. For MeOH, **Cat1**^{OTf} experimentally provided higher catalytic effect than **Cat2**^{OTf}, whereas the calculated $\Delta G^{\neq}$ for **Cat1**$^+$ is higher than that for **Cat2**$^+$-catalyzed process (61.1 kJ mol^{-1} vs 49.1 kJ mol^{-1}, respectively). Such the difference between the experiment and theoretical consideration may be explained by the different equilibrium concentration of the activated form of the aldehyde (**A•Cat**). Indeed, for the **Cat1**^{OTf} species the obtained computational data indicate nearly selective association of **Cat1**$^+$ with the aldehyde **A** (–9.3 kJ mol^{-1} for **A•1** vs 12.0 kJ mol^{-1} for **B•1**), whereas **Cat2**$^+$ binds the reaction substrates significantly less selectively (–8.2 kJ mol^{-1} for **A•2** vs 0.5 kJ mol^{-1} for **B•2**).

Conclusions

In this work, it was shown experimentally that the catalytic activity of σ-hole donating organocatalysts cannot be clearly predicted neither from the analysis of catalyst···TS intermolecular interactions nor from the value of reduction of the Gibbs free energy of activation of the reaction. Solvation effects and other competitive binding processes play at least the same or even more important role in the catalysis.

During the reaction progress, the catalyst reversibly associates with a target electrophilic species thus accelerating the reaction due to the electrophilic activation, as well as binds the nucleophile giving inactive Cat···Nu species. Such an equilibrium in great extent is caused by the solvation effects and rational choice of the solvent is required for the catalyst to fully display its catalytic ability (**Scheme 4, *a***). One of the ways to solve this problem is utilization of the solvents exhibiting high affinity to the nucleophile, which will compete with the catalyst in the binding with the nucleophile. In the simplest case, this approach should shift the equilibrium to the reactive Cat···electrophile species but reduce the activity of the "unbound" nucleophile. Such an effect can be observed in this work by analysis of the experimental and computational data for **Cat3**^{OTf}-catalyzed forward reaction rate constant in MeCN (k_{-1} = 13×10^{-3} M^{-1} s^{-1}; $\Delta\Delta G_{binding}$ = 1 kJ mol^{-1}) and MeOH (k_{-1} = 1.7×10^{-3} M^{-1} s^{-1}; $\Delta\Delta G_{binding}$ = –11.1 kJ mol^{-1}), where the forward reaction is slower in MeOH although the estimated equilibrium concentration of the Cat···electrophile associates is higher in this solvent.

Rational structural design of the catalysts providing their higher affinity to the electrophilic species (**Scheme 4, *b***) or discriminating binding to the nucleophile (**Scheme 4, *c***) seems to be more complex but effective approach. Incorporation in the catalyst structure of the side-groups providing additional van der Waals interactions as well as hydrogen-, pnictogen-, chalcogen-, or halogen bonds with the electrophile or steric/electrostatic repulsion from the nucleophile is the way to reach this goal.

We hope that this study, on the one hand, sheds light on the importance of complex association processes taking place in the progress of reactions catalyzed by the ChB or XB donors, which can drastically affect the catalytic activity of the organocatalysts and, on the other hand, sets the direction for further consideration of the side-interactions between the catalysts and reaction substrates, which can modulate their binding selectivity. The computational model utilized in this work and the obtained results also might be useful in the field of noncovalent ion and molecular recognition, which recently has been extensively realized utilizing ChB and XB donors.[2, 16, 24, 57-59]

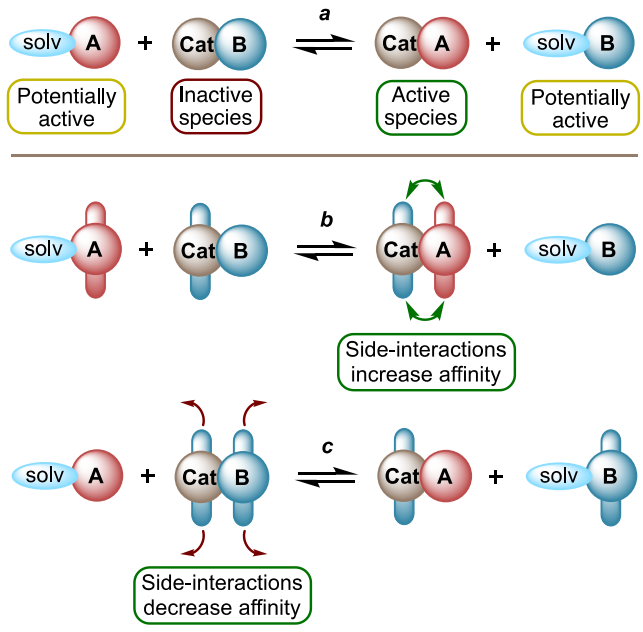

Scheme 4. Equilibrium between active and inactive catalyst···substrate associates.

Experimental Section

Materials and instrumentation. All solvents, *tert*-butylamine and 4-methylbenzaldehyde were obtained from commercial sources and used as received. The catalysts **Cat1**^{OTf}–**Cat3**^{OTf} were synthesized according to published procedures with some modifications.[40, 60, 61] All syntheses were conducted in air. Chromatographic separation was carried out using Macherey-Nagel silica gel 60 M (0.063–0.2 mm). Melting points were measured on a Stuart SMP30 apparatus in capillaries and are not corrected. Electrospray ionization mass-spectra were obtained on a Bruker maXis spectrometer equipped with an electrospray ionization (ESI) source. The instrument was operated in positive ion mode using an *m*/*z* range 50–1200. The nebulizer gas flow was 1.0 bar and the drying gas flow 4.0 L min^{-1}. For HRESI$^+$, the studied compounds were dissolved in MeOH. ^{1}H- and ^{13}C{^{1}H} NMR spectra were measured on a Bruker Avance 400 and Bruker Avance 500 spectrometers in $CDCl_3$, $(CD_3)_2SO$, CD_3OD at 298 K; the residual solvent signal was used as the internal standard.

^{1}H NMR monitoring of the modelled reaction. A solution of *tert*-butylamine (10.5 μL, 0.1 mmol) in CD_3CN, $(CD_3)_2SO$ or CD_3OD (300 μL) was added to a mixture of 4-methylbenzaldehyde (0.1 mmol) and the catalyst **Cat1**^{OTf}–**Cat3**^{OTf} (0.01 mmol) or without catalyst dissolved in the corresponding solvent and placed in an NMR tube. The closed NMR tube was shaken 3 times, immediately placed in an NMR spectrometer, and the ^{1}H NMR spectra were recorded every 2 min (four scans; repetition time = 4 s) for 2 h at 298 K. The reaction progress was monitored by measuring the time-dependent integral intensity of the proton signals in aldehyde and imine groups (see **Supporting Information**).

Computational details. The full geometry optimization of all model structures was carried out at the DFT level of theory using the M06-2X functional[62] with the help of the Gaussian-09 program package.[63] The M06-2X functional was specifically developed and parameterized for a correct description of noncovalent interactions and thermochemistry (especially in the case of main group chemical elements)[62] and was also validated for these purposes in several benchmark studies.[64-66] We have chosen this functional according to our previous experience and its successful performance in a number of halogen and chalcogen bonds studies in various similar supramolecular systems and organocatalysis processes.[42, 47, 67] The quasi-relativistic MWB46 pseudopotentials,[68] which described 46 core electrons, and the appropriate contracted basis sets were used for I atoms, while the standard 6-31G* basis sets were used for all other atoms. No symmetry restrictions were applied during the geometry optimizations. The Hessian matrices were calculated analytically for all optimized model structures to prove the location of the correct minimum or saddle point on the potential energy surface (no imaginary frequencies or only one imaginary frequency, respectively). The Cartesian atomic coordinates for all model structures are presented in xyz-file (see **Supporting Information**).

Conflicts of interest

There are no conflicts to declare.

Acknowledgements

This work was supported by the Russian Science Foundation (grant 20-73-10013). Physicochemical studies were performed at the Center for Magnetic Resonance, Chemistry Educational Centre, and Center for Chemical Analysis and Materials Research (all at Saint Petersburg State University).

References

1. G. Cavallo, P. Metrangolo, R. Milani, T. Pilati, A. Priimagi, G. Resnati and G. Terraneo, The Halogen Bond, *Chem. Rev.*, 2016, **116**, 2478–2601.

2. L. Vogel, P. Wonner and S. M. Huber, Chalcogen Bonding: An Overview, *Angew. Chem. Int. Ed.*, 2019, **58**, 1880-1891.

3. O. García Mancheño and M. Waser, Recent Developments and Trends in Asymmetric Organocatalysis, *Eur. J. Org. Chem.*, 2022, **2022**, e202200950.

4. P. Peluso and V. Mamane, Stereoselective Processes Based on sigma-Hole Interactions, *Molecules*, 2022, **27**, 4625.

5. C. M. Volla, I. Atodiresei and M. Rueping, Catalytic C-C bond-forming multi-component cascade or domino reactions: pushing the boundaries of complexity in asymmetric organocatalysis, *Chem. Rev.*, 2014, **114**, 2390–2431.

6. F. E. Held and S. B. Tsogoeva, Asymmetric cycloaddition reactions catalyzed by bifunctional thiourea and squaramide organocatalysts: recent advances, *Catal. Sci. Technol.*, 2016, **6**, 645–667.

7. K. Takagi, H. Murakata and T. Hasegawa, Application of Thiourea/Halogen Bond Donor Cocatalysis in Metal-Free Cationic Polymerization of Isobutyl Vinyl Ether and Styrene Derivatives, *Macromolecules*, 2022, **55**, 5756-5765.

8. P. Wonner, A. Dreger, L. Vogel, E. Engelage and S. M. Huber, Chalcogen Bonding Catalysis of a Nitro-Michael Reaction, *Angew. Chem. Int. Ed.*, 2019, **58**, 16923–16927.

9. V. Oliveira, M. Cardoso and L. Forezi, Organocatalysis: A Brief Overview on Its Evolution and Applications, *Catalysts*, 2018, **8**, 605.

10. Y. Qin, L. Zhu and S. Luo, Organocatalysis in Inert C-H Bond Functionalization, *Chem. Rev.*, 2017, **117**, 9433–9520.

11. X. Han, H. B. Zhou and C. Dong, Applications of Chiral Squaramides: From Asymmetric Organocatalysis to Biologically Active Compounds, *Chem. Rec.*, 2016, **16**, 897–906.

12. T. James, M. van Gemmeren and B. List, Development and Applications of Disulfonimides in Enantioselective Organocatalysis, *Chem. Rev.*, 2015, **115**, 9388–9409.

13. B. Han, X. H. He, Y. Q. Liu, G. He, C. Peng and J. L. Li, Asymmetric organocatalysis: an enabling technology for medicinal chemistry, *Chem. Soc. Rev.*, 2021, **50**, 1522–1586.

14. A. S. Novikov and D. S. Bolotin, Halonium, chalconium, and pnictonium salts as noncovalent organocatalysts: a computational study on relative catalytic activity, *Org. Biomol. Chem.*, 2022, **20**, 7632–7639.

15. S. Kolb, G. A. Oliver and D. B. Werz, Chemistry Evolves, Terms Evolve, but Phenomena Do Not Evolve: From Chalcogen-Chalcogen Interactions to Chalcogen Bonding, *Angew. Chem. Int. Ed.*, 2020, **59**, 22306–22310.

16. J. Y. C. Lim and P. D. Beer, Sigma-Hole Interactions in Anion Recognition, *Chem*, 2018, **4**, 731–783.

17. D. Bulfield and S. M. Huber, Halogen Bonding in Organic Synthesis and Organocatalysis, *Chem.–Eur. J.*, 2016, **22**, 14434–14450.

18. F. Heinen, E. Engelage, A. Dreger, R. Weiss and S. M. Huber, Iodine(III) Derivatives as Halogen Bonding Organocatalysts, *Angew. Chem. Int. Ed.*, 2018, **57**, 3830–3833.

19. R. L. Sutar and S. M. Huber, Catalysis of Organic Reactions through Halogen Bonding, *ACS Catal.*, 2019, **9**, 9622–9639.

20. K. Strakova, L. Assies, A. Goujon, F. Piazzolla, H. V. Humeniuk and S. Matile, Dithienothiophenes at Work: Access to Mechanosensitive Fluorescent Probes, Chalcogen-Bonding Catalysis, and Beyond, *Chem. Rev.*, 2019, **119**, 10977–11005.

21. S. Benz, J. Mareda, C. Besnard, N. Sakai and S. Matile, Catalysis with chalcogen bonds: neutral benzodiselenazole scaffolds with high-precision selenium donors of variable strength, *Chem. Sci.*, 2017, **8**, 8164-8169.

22. N. Tarannam, M. H. H. Voelkel, S. M. Huber and S. Kozuch, Chalcogen vs Halogen Bonding Catalysis in a Water-Bridge-Cocatalyzed Nitro-Michael Reaction, *J. Org. Chem.*, 2022, **87**, 1661–1668.

23. P. Wonner, T. Steinke, L. Vogel and S. M. Huber, Carbonyl Activation by Selenium- and Tellurium-Based Chalcogen Bonding in a Michael Addition Reaction, *Chem.–Eur. J.*, 2020, **26**, 1258–1262.

24. N. Biot and D. Bonifazi, Chalcogen-bond driven molecular recognition at work, *Coord. Chem. Rev.*, 2020, **413**, 213243.

25. K. T. Mahmudov, M. N. Kopylovich, M. F. C. Guedes da Silva and A. J. L. Pombeiro, Chalcogen bonding in synthesis, catalysis and design of materials, *Dalton Trans.*, 2017, **46**, 10121–10138.

26. T. Steinke, P. Wonner, R. M. Gauld, S. Heinrich and S. M. Huber, Catalytic Activation of Imines by Chalcogen Bond Donors in a Povarov [4+2] Cycloaddition Reaction, *Chem.–Eur. J.*, 2022, **28**, e202200917.

27. H. Zhu, P. P. Zhou and Y. Wang, Cooperative chalcogen bonding interactions in confined sites activate aziridines, *Nat. Commun.*, 2022, **13**, 3563.

28. K. Chen, R. Yan, Z. Li, W. Huang, L. Gao, T. Duan, H. Tong, Y. Li, J. Sun and K. Guo, Halogen bonding catalysis for the [3+2] cycloaddition reactions of epoxides with CO2, and other heterocumulenes, *J. CO_2 Util.*, 2021, **52**.

29. S. Portela, J. J. Cabrera-Trujillo and I. Fernandez, Catalysis by Bidentate Iodine(III)-Based Halogen Donors: Surpassing the Activity of Strong Lewis Acids, *J. Org. Chem.*, 2021, **86**, 5317–5326.

30. R. Robidas, D. L. Reinhard, C. Y. Legault and S. M. Huber, Iodine(III)-Based Halogen Bond Donors: Properties and Applications, *Chem. Rec.*, 2021, **21**, 1912–1927.

31. F. Heinen, E. Engelage, C. J. Cramer and S. M. Huber, Hypervalent Iodine(III) Compounds as Biaxial Halogen Bond Donors, *J. Am. Chem. Soc.*, 2020, **142**, 8633–8640.

32. D. L. Reinhard, F. Heinen, J. Stoesser, E. Engelage and S. M. Huber, Tuning the Halogen Bonding Strength of Cyclic Diaryliodonium Salts, *Helv. Chim. Acta*, 2021, **104**, e2000221.

33. A. Boelke, T. J. Kuczmera, E. Lork and B. J. Nachtsheim, N-Heterocyclic Iod(az)olium Salts - Potent Halogen-Bond Donors in Organocatalysis, *Chem.–Eur. J.*, 2021, **27**, 13128–13134.

34. F. Heinen, D. L. Reinhard, E. Engelage and S. M. Huber, A Bidentate Iodine(III)-Based Halogen-Bond Donor as a Powerful Organocatalyst, *Angew. Chem. Int. Ed.*, 2021, **60**, 5069–5073.

35. R. J. Mayer, A. R. Ofial, H. Mayr and C. Y. Legault, Lewis Acidity Scale of Diaryliodonium Ions toward Oxygen, Nitrogen, and Halogen Lewis Bases, *J. Am. Chem. Soc.*, 2020, **142**, 5221–5233.

36. A. Labattut, P. L. Tremblay, O. Moutounet and C. Y. Legault, Experimental and Theoretical Quantification of the Lewis Acidity of Iodine(III) Species, *J. Org. Chem.*, 2017, **82**, 11891–11896.

37. Y. Nishida, T. Suzuki, Y. Takagi, E. Amma, R. Tajima, S. Kuwano and T. Arai, A Hypervalent Cyclic Dibenzoiodolium Salt as a Halogen-Bond-Donor Catalyst for the [4+2] Cycloaddition of 2-Alkenylindoles, *ChemPlusChem*, 2021, **86**, 741–744.

38. Y. Zhang, J. Han and Z.-J. Liu, Diaryliodonium salts as efficient Lewis acid catalysts for direct three component Mannich reactions, *RSC Adv.*, 2015, **5**, 25485–25488.

39. R. Haraguchi, T. Nishikawa, A. Kanazawa and S. Aoshima, Metal-Free Living Cationic Polymerization Using

Diaryliodonium Salts as Organic Lewis Acid Catalysts, *Macromolecules*, 2020, **53**, 4185–4192.

40. S. N. Yunusova, A. S. Novikov, N. S. Soldatova, M. A. Vovk and D. S. Bolotin, Iodonium salts as efficient iodine(iii)-based noncovalent organocatalysts for Knorr-type reactions, *RSC Adv.*, 2021, **11**, 4574–4583.

41. A. S. Novikov and D. S. Bolotin, Xenon Derivatives as Aerogen Bond-Donating Catalysts for Organic Transformations: A Theoretical Study on the Metaphorical "Spherical Cow in a Vacuum" Provides Insights into Noncovalent Organocatalysis, *J. Org. Chem.*, 2022, DOI: 10.1021/acs.joc.2c00680, in press.

42. M. V. Il'in, A. A. Sysoeva, A. S. Novikov and D. S. Bolotin, Diaryliodoniums as Hybrid Hydrogen- and Halogen-Bond-Donating Organocatalysts for the Groebke-Blackburn-Bienayme Reaction, *J. Org. Chem.*, 2022, **87**, 4569–4579.

43. A. Boelke, T. J. Kuczmera, L. D. Caspers, E. Lork and B. J. Nachtsheim, Iodolopyrazolium Salts: Synthesis, Derivatizations, and Applications, *Org. Lett.*, 2020, **22**, 7261–7266.

44. B. Zhou and F. P. Gabbai, Anion Chelation via Double Chalcogen Bonding: The Case of a Bis-telluronium Dication and Its Application in Electrophilic Catalysis via Metal-Chloride Bond Activation, *J. Am .Chem. Soc.*, 2021, **143**, 8625–8630.

45. R. Weiss, E. Aubert, P. Pale and V. Mamane, Chalcogen-Bonding Catalysis with Telluronium Cations, *Angew. Chem. Int. Ed.*, 2021, **60**, 19281–19286.

46. R. Robidas, D. L. Reinhard, S. M. Huber and C. Y. Legault, A Quantum-chemical Analysis on the Lewis Acidity of Diarylhalonium Ions, *ChemPhysChem*, 2022, e202200634.

47. D. A. Polonnikov, M. V. Il'in, Y. V. Safinskaya, I. S. Aliyarova, A. S. Novikov and D. S. Bolotin, (Pre)association as a crucial step for computational prediction and analysis of the catalytic activity of σ-hole donating organocatalysts, *Org. Chem. Front.*, 2023, DOI: 10.1039/d2qo01648f.

48. D. Kaiser, I. Klose, R. Oost, J. Neuhaus and N. Maulide, Bond-Forming and -Breaking Reactions at Sulfur(IV): Sulfoxides, Sulfonium Salts, Sulfur Ylides, and Sulfinate Salts, *Chem. Rev.*, 2019, **119**, 8701–8780.

49. Y. Lu, Q. Liu, Z. X. Wang and X. Y. Chen, Alkynyl Sulfonium Salts Can Be Employed as Chalcogen-Bonding Catalysts and Generate Alkynyl Radicals under Blue-Light Irradiation, *Angew. Chem. Int. Ed.*, 2022, **61**, e202116071.

50. S. S. Karandikar, A. Bhattacharjee, B. E. Metze, N. Javaly, E. J. Valente, T. M. McCormick and D. R. Stuart, Orbital analysis of bonding in diarylhalonium salts and relevance to periodic trends in structure and reactivity, *Chem. Sci.*, 2022, **13**, 6532–6540.

51. A. Y. Bastidas Angel, P. R. O. Campos and E. E. Alberto, Synthetic application of chalcogenonium salts: beyond sulfonium, *Org. Biomol. Chem.*, 2023, DOI: 10.1039/d2ob01822e.

52. Y. Yoshida, T. Fujimura, T. Mino and M. Sakamoto, Chiral Binaphthyl-Based Iodonium Salt (Hypervalent Iodine(III)) as Hydrogen- and Halogen-Bonding Bifunctional Catalyst: Insight into Abnormal Counteranion Effect and Asymmetric Synthesis of N,S-Acetals, *Adv. Synth. Catal.*, 2022, **364**, 1091–1098.

53. T. Chivers and R. S. Laitinen, Tellurium: a maverick among the chalcogens, *Chem. Soc. Rev.*, 2015, **44**, 1725–1739.

54. V. K. Burianova, D. S. Bolotin, A. S. Mikherdov, A. S. Novikov, P. P. Mokolokolo, A. Roodt, V. P. Boyarskiy, D. Dar'in, M. Krasavin, V. V. Suslonov, A. P. Zhdanov, K. Y. Zhizhin and N. T. Kuznetsov, Mechanism of generation of closo-decaborato amidrazones. Intramolecular non-covalent B–H···π(Ph) interaction determines stabilization of the configuration around the amidrazone C=N bond, *New J. Chem.*, 2018, **42**, 8693–8703.

55. M. V. Il'in, A. S. Novikov and D. S. Bolotin, Sulfonium and Selenonium Salts as Noncovalent Organocatalysts for the Multicomponent Groebke-Blackburn-Bienayme Reaction, *J. Org. Chem.*, 2022, **87**, 10199-10207.

56. D. S. Bolotin, V. K. Burianova, A. S. Novikov, M. Y. Demakova, C. Pretorius, P. P. Mokolokolo, A. Roodt, N. A. Bokach, V. V. Suslonov, A. P. Zhdanov, K. Y. Zhizhin, N. T. Kuznetsov and V. Y. Kukushkin, Nucleophilicity of Oximes Based upon Addition to a Nitrilium *closo*-Decaborate Cluster, *Organometallics*, 2016, **35**, 3612–3623.

57. A. Docker, C. H. Guthrie, H. Kuhn and P. D. Beer, Modulating Chalcogen Bonding and Halogen Bonding Sigma-Hole Donor Atom Potency and Selectivity for Halide Anion Recognition, *Angew. Chem. Int. Ed.*, 2021, **60**, 21973–21978.

58. M. S. Taylor, Anion recognition based on halogen, chalcogen, pnictogen and tetrel bonding, *Coord. Chem. Rev.*, 2020, **413**, 213270.

59. R. Tepper and U. S. Schubert, Halogen Bonding in Solution: Anion Recognition, Templated Self-Assembly, and Organocatalysis, *Angew. Chem. Int. Ed.*, 2018, **57**, 6004–6016.

60. P. Xu, D. Zhao, F. Berger, A. Hamad, J. Rickmeier, R. Petzold, M. Kondratiuk, K. Bohdan and T. Ritter, Site-Selective Late-Stage Aromatic [18F]Fluorination via Aryl Sulfonium Salts, *Angew. Chem. Int. Ed.*, 2020, **59**, 1956–1960.

61. S.-i. Watanabe, K. Yamamoto, Y. Itagaki, T. Iwamura, T. Iwama and T. Kataoka, The First Aryne Evolution from the Reactions of Selenonium Salts with Aryllithiums, *Tetrahedron*, 2000, **56**, 855–863.

62. Y. Zhao and D. G. Truhlar, The M06 suite of density functionals for main group thermochemistry, thermochemical kinetics, noncovalent interactions, excited states, and transition elements: two new functionals and systematic testing of four M06-class functionals and 12 other functionals, *Theor. Chem. Acc.*, 2007, **120**, 215–241.

63. M. J. Frisch, G. W. Trucks, H. B. Schlegel, G. E. Scuseria, M. A. Robb, J. R. Cheeseman, G. Scalmani, V. Barone, B. Mennucci, G. A. Petersson, H. Nakatsuji, M. Caricato, X. Li, H. P. Hratchian, A. F. Izmaylov, J. Bloino, G. Zheng, J. L. Sonnenberg, M. Hada, M. Ehara, K. Toyota, R. Fukuda, J. Hasegawa, M. Ishida, T. Nakajima, Y. Honda, O. Kitao, H. Nakai, T. Vreven, J. J. A. Montgomery, J. E. Peralta, F. Ogliaro, M. Bearpark, J. J. Heyd, E. Brothers, K. N. Kudin, V. N. Staroverov, T. Keith, R. Kobayashi, J. Normand, K. Raghavachari, A. Rendell, J. C. Burant, S. S. Iyengar, J. Tomasi, M. Cossi, N. Rega, J. M. Millam, M. Klene, J. E. Knox, J. B. Cross, V. Bakken, C. Adamo, J. Jaramillo, R. Gomperts, R. E. Stratmann, O. Yazyev, A. J. Austin, R. Cammi, C. Pomelli, J. W. Ochterski, R. L. Martin, K. Morokuma, V. G. Zakrzewski, G. A. Voth, P. Salvador, J. J. Dannenberg, S. Dapprich, A. D. Daniels, O. Farkas, J. B. Foresman, J. V. Ortiz, J. Cioslowski and D. J. Fox, Gaussian 09, Revision C.01, 2010.

64. A. Bauza, I. Alkorta, A. Frontera and J. Elguero, On the Reliability of Pure and Hybrid DFT Methods for the Evaluation of Halogen, Chalcogen, and Pnicogen Bonds Involving Anionic and Neutral Electron Donors, *J. Chem. Theory. Comput.*, 2013, **9**, 5201–5210.

65. N. Mardirossian and M. Head-Gordon, How Accurate Are the Minnesota Density Functionals for Noncovalent Interactions, Isomerization Energies, Thermochemistry, and Barrier Heights Involving Molecules Composed of Main-Group Elements?, *J. Chem. Theory Comput.*, 2016, **12**, 4303–4325.

66. Y. Wang, P. Verma, X. Jin, D. G. Truhlar and X. He, Revised M06 density functional for main-group and transition-metal chemistry, *Proc. Natl. Acad. Sci. U. S. A.*, 2018, **115**, 10257–10262.

67. A. A. Sysoeva, A. S. Novikov, M. V. Il'in, V. V. Suslonov and D. S. Bolotin, Predicting the catalytic activity of

azolium-based halogen bond donors: an experimentally-verified theoretical study, *Org. Biomol. Chem.*, 2021, **19**, 7611–7620.

68. A. Bergner, M. Dolg, W. Küchle, H. Stoll and H. Preuß, Ab initio energy-adjusted pseudopotentials for elements of groups 13–17, *Mol. Phys.*, 1993, **80**, 1431–1441.